Relation between n-value and critical current in filamentary and coated superconducting tapes with tensile stress-induced cracks

AUTHOR(S):

Ochiai, Shojiro; Okuda, Hiroshi; Fujimoto, Masahiro; Osamura, Kozo

CITATION:

Ochiai, Shojiro ...[et al]. Relation between n-value and critical current in filamentary and coated superconducting tapes with tensile stress-induced cracks. Materials Transactions 2015, 56(9): 1558-1564

ISSUE DATE:

2015-09-01

URL:

http://hdl.handle.net/2433/250427

Materials Transactions, Vol. 56, No. 9 (2015) pp. 1558 to 1564

Relation between *n*-Value and Critical Current in Filamentary and Coated Superconducting Tapes with Tensile Stress-Induced Cracks

Shojiro Ochiai[1], Hiroshi Okuda[2], Masahiro Fujimoto[2,*] and Kozo Osamura[3]

[1]*Elements Strategy Initiative for Structural Materials, Kyoto University, Kyoto 606-8501, Japan*
[2]*Department of Materials Science and Engineering, Kyoto University, Kyoto 606-8501, Japan*
[3]*Research Institute for Applied Sciences, Kyoto 606-8202, Japan*

We have determined experimentally that the *n*-value of tension-damaged bismuth strontium calcium copper oxide (BSCCO, Bi2223) filamentary superconducting tape decreases very sharply with decreasing critical current, compared with bending-damaged tape. In this work, the sharp decrease in the *n*-value associated with decreasing critical current under applied tensile stress/strain was studied with a current shunting model that assumes cracks in filamentary and coated superconductors. In a filamentary conductor containing collective filament cracks, defined as cracks composed of successively cracked filaments in a transverse cross-section, the decrease in the cross-sectional area of the superconducting current transportable-filaments reduces the critical current, and the shunting current at the crack reduces the *n*-value. In addition, the decrease in the electrical resistance in the current shunting circuit increases the critical current slightly and decreases the *n*-value sharply. The experimentally measured relationship between the *n*-value and the critical current for two BSCCO samples from different manufacturers was described by the upper and lower bounds calculated with the current shunting circuit resistance as a variable. The experimentally measured relationship between the *n*-value and the critical current for two different coated conductors were described in a similar manner.
[doi:10.2320/matertrans.MAW201501]

(Received April 1, 2015; Accepted June 29, 2015; Published August 7, 2015)

Keywords: *superconducting tape, crack, critical current, n-value, modeling analysis, shunting current*

1. Introduction

In multi-filamentary composite tapes under tensile stress/strain, the weaker filaments in the gauge length crack at an early stage. Subsequently, the stress concentration arising from the cracked filaments causes collective cracks, which are composed of successively cracked filaments in a transverse cross-section,[1–3] dramatically reducing the critical current and *n*-value. Under bending strain, filament cracking is caused by the tensile strain in the length direction, although its extent depends on the location in this direction.[4–8] In addition, the tensile strain varies greatly along the thickness direction; it is equal to the residual strain at the neutral axis, and it increases with distance from the neutral axis on the tensile side. Accordingly, the filaments far from the neutral axis are cracked severely, whereas those near the neutral axis are less cracked.

Due to the difference in damage evolution between tensile stress/strain and bending strain,[6] the relationship between *n*-value and critical current (I_c) measured under tensile stress/strain is different from that measured under bending strain. Figure 1 shows the experimental results for two bismuth strontium calcium copper oxide (BSCCO:Bi2223) filamentary tape samples (Samples A and B) supplied by different manufacturers. For both samples, the voltage-current (*V*-*I*) curves at various applied tensile stresses/bending strains were measured for a distance between the voltage taps (L) of 1 cm. The values of critical current (I_c) were obtained with an electric field criterion of $E_c = 1\,\mu V/cm$, corresponding to $V_c = E_c L = 1\,\mu V$ in this case, and the *n*-values were obtained as the *n*-index in $V \propto I^n$ for the electric field range of $E = 0.1$–$10\,\mu V/cm$, corresponding to the voltage range of $V = 0.1$–$10\,\mu V$. The *n*-value given by $\partial \ln(V)/\partial \ln(I)$ refers to the slope of the *V*-*I* curve in the voltage range of $V = 0.1$–

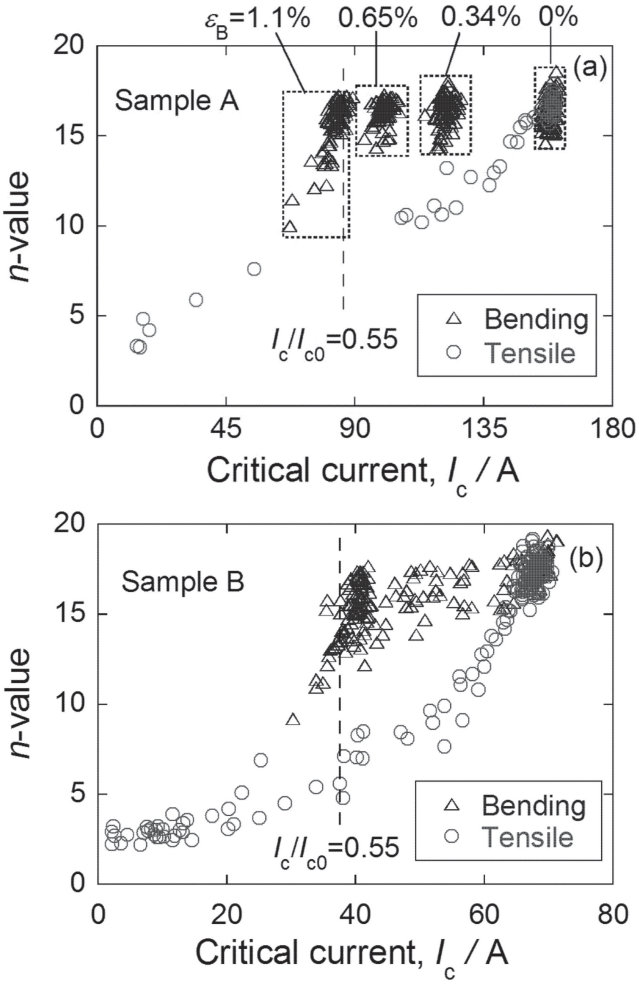

Fig. 1 *n*-value as a function of I_c measured under tensile stress and under bending strain in two BSCCO(Bi2223) filamentary tape samples supplied by different manufacturers; (a) Sample A and (b) Sample B. The data for Sample A under tensile stress[1] and bending strain[5] and those of Sample B under tensile stress[6] and bending strain[7] were taken from our previous work.

*Graduate Student, Kyoto University

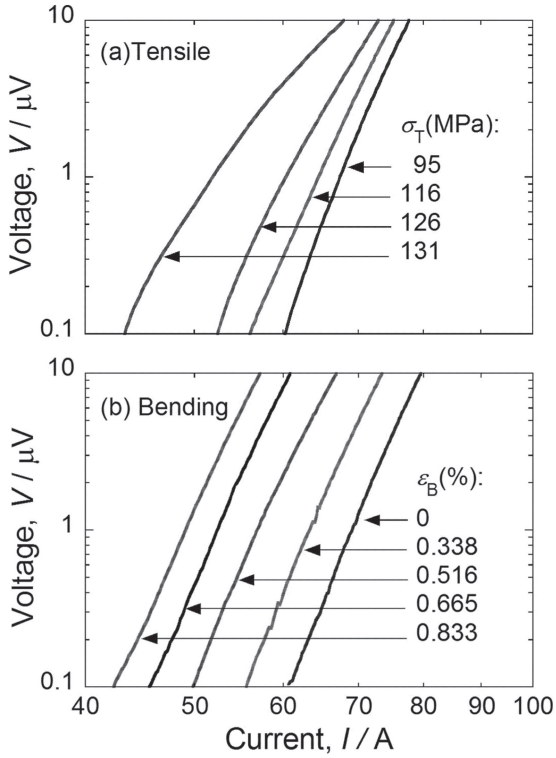

Fig. 2 Examples of the V-I curves of Sample B (BSCCO filamentary sample) under applied (a) tensile stress, σ_T, and (b) bending strain, ε_B.

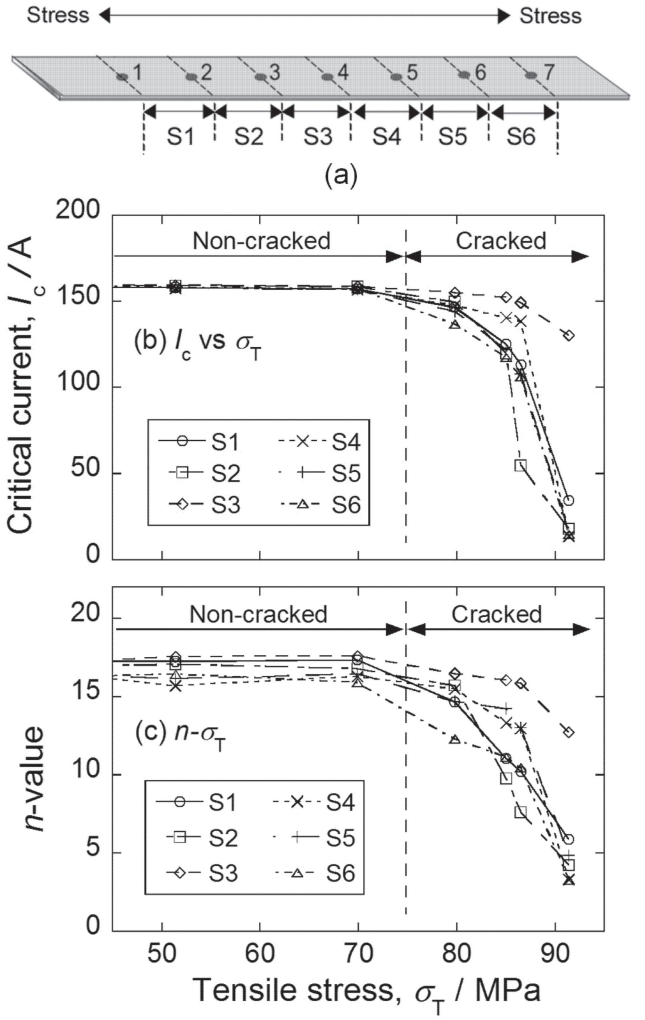

Fig. 3 (a) Configuration of the test piece for measuring the I_c and n-value of Samples A and B under applied tensile stress, σ_T. (b), (c) Experimental results for Sample A showing the change in I_c and n-value with increase in applied stress.[1] The I_c and n-value were measured for sections S1 to S6 in the test piece in (a). Because σ_T was the same in S1 to S6 in this test piece, the I_c and n-value measured for S1 to S6 are plotted against σ_T in (b) and (c).

10 μV on the logarithmic scale. The V-I curves, which are straight for the logarithmic scale when the samples are not damaged, become curved when samples are damaged under tensile stress/strain. In this case, the n-value is estimated as the average slope in the corresponding electric field range. The data for Sample A (Fig. 1(a)) were taken from Refs. 1) and 5), and those for Sample B (Fig. 1(b)) from Refs. 6) and 7). The following features were observed. (1) Under no applied stress, the average critical current value, I_{c0}, and average n-value, n_0, are 158 A and 17 for Sample A, and 68 A and 17 for Sample B, respectively. In the range of $I_c/I_{c0} > 0.55$ in Fig. 1, the decrease in n-value with decreasing I_c under bending strain is small compared with that under tensile stress. (2) In the range of $I_c/I_{c0} < 0.55$, the decrease in n-value with decreasing I_c under bending strain becomes very sharp. This behavior could be attributed to the filaments buckling on the compression side and damage on the tension side.[5,7,9]

Feature (1) is visible as the difference in the shape of the V-I curves on the logarithmic scale in Fig. 2. The n-value decreases sharply with decreasing I_c under tension in the representative curves of Sample B in the current region of $I_c/I_{c0} > 0.55$, although it decreases slightly under bending (Fig. 1(b)). The average slope $(\partial \ln(V)/\partial \ln(I))$ in the range of $V = 0.1$–10 μV in Fig. 2, corresponding to the n-value, decreases with increasing tensile stress. In contrast, under bending strain, the decrease in slope is slight.

In our recent work,[6] we described the slight decrease in n-value with decreasing I_c under bending strain in the I_c range of $I_c/I_{c0} > 0.55$ before buckling in Sample B. The model described the experimental results for the location-dependent damage evolution in the sample thickness direction. In the present work, we focus on describing the sharp decrease in n-value with decreasing I_c under tensile stress/strain.

In our measurements of the I_c and n-value of Sample A under tension,[1] seven voltage taps were attached to the tape surface spaced at intervals (L) of 1 cm (Fig. 3(a)), and the V-I curves of the six sections (S1 to S6) with a length of 1 cm were measured under various tensile stresses. Because of the difference in cracking behavior among the sections, the strains of the sections were different although the stress was the same. Therefore, stress σ_T is used instead of strain as a measure of the mechanical conditions under tension. The change in I_c and n-value of S1 to S6 with applied stress are shown in Fig. 3(b) and (c). The I_c and n-value remain nearly constant up to $\sigma_T = 69.9$ MPa. Above $\sigma_T = 79.8$ MPa, both I_c and n-value decrease with increasing σ_T because of the Bi2223 filaments cracking. The boundary between non-cracked and cracked regions is indicated with broken lines. The crack evolution behavior is different for S1 to S6, even under the same σ_T. This feature is reflected in the large difference in the change in I_c and n-value with σ_T among S1 to S6.

In our recent work, a current shunting model of the cracked region[10–12] described the *V-I* curves and change in I_c and *n*-value with increasing applied tensile stress in Sample A satisfactorily.[1] The model is described in Subsection 2.1. Under tensile stress/strain, I_c and *n*-value are affected by the crack density and crack size distribution; *n*-value tends to be higher for higher crack densities and narrow crack size distribution.[13–15] Furthermore, different *n*-values can co-exist for a value of I_c. This implies that the relationship between *n*-value and I_c is not uniquely determined because crack evolution is different among samples. In this work, to overcome this problem, we used the current shunting model to provide the upper and lower bounds to calculate the *n*-I_c relation. The calculations based on the current shunting model are described in Subsection 2.2. We applied our approach to describing the experimental results for a filamentary conductor (Samples A and B under tension in Fig. 1). Furthermore, the present approach was used to calculate the *n*-I_c relationship for coated conductors, which show a sharp decrease in *n*-value with decreasing critical current under tension,[11–15] similarly to that in filamentary conductors. The results obtained by the present approach for filamentary and coated conductors are shown in Subsections 3.1 and 3.2, respectively.

2. Calculation of the *n*-I_c Relation

2.1 Current shunting model in cracked region

Figure 4 shows a schematic representation of the (a) current path and (b) simplified electrical circuit in collective cracks in filamentary conductors, based on the partial crack-current shunting model.[1,10–15] A partial crack is defined as a crack that exists in part of the transverse cross-section of the superconducting filament or layer. Similar to our previous work,[1] Bi2223 filaments are replaced by a single equivalent filament and the collective cracks are replaced by a single equivalent partial crack. Moreover, in our previous analysis of the *V-I* curve, I_c, and *n*-value of cracked coated conductors,[11–15] we replaced the arrayed multiple cracks with a single equivalent crack in the model, because current shunting occurs via the same mechanism in both single and multiple cracks. The experimental results were described well despite the replacement, suggesting that replacement is a useful analysis tool. Based on this finding, we also use the single equivalent crack model in this work. As shown later, the experimental results for filamentary and coated conductors are well described by the present approach.

In this subsection, a filamentary conductor is used to illustrate a model that can be applied to both filamentary and coated conductors. f is the ratio of the cross-sectional area of the cracked part to the total cross-sectional area of the filament and $1-f$ is the area ratio of the ligament. The ligament with area ratio $1-f$ transports current I_b. In the cracked part with area ratio f, current I_s ($= I - I_b$) is shunted into Ag. The voltage that develops in the ligament that transports current I_b, is denoted as V_b in Fig. 4(b). The voltage, $V_s = I_s R_t$ (R_t is the current shunting circuit resistance, I_s is the shunting current), that develops in the cracked part from I_s, is equal to V_b because the ligament and cracked parts

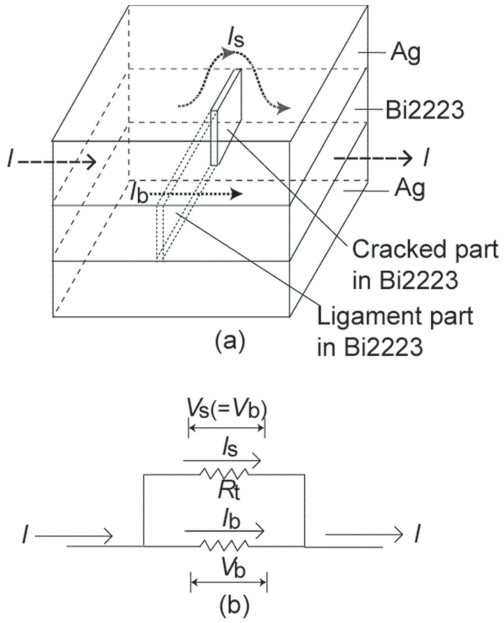

Fig. 4 Schematic of (a) current path and (b) simplified electrical circuit for an existing partial crack.

form a parallel circuit. Thus, we can express the *V-I* relation of cracked sample as[1,11–15]

$$V = E_c L \left(\frac{I}{I_{c0}}\right)^{n_0} + V_b \tag{1}$$

$$I = I_b + I_s = I_{c0}(1-f)\left(\frac{L}{s}\right)^{\frac{1}{n_0}}\left[\frac{V_b}{E_c L}\right]^{\frac{1}{n_0}} + \frac{V_b}{R_t} \tag{2}$$

where L ($= 1$ cm) is the distance between the voltage taps, s is the current transfer length,[14] I_{c0} is the critical current of the non-cracked Bi2223 conductor, and n_0 is the *n*-value in the non-cracked state. Fang *et al.*[10] used s as the opening displacement of the crack although it can be replaced by the current transfer length, from which eqs. (1) and (2) can be derived in the same manner. When the values of $(1-f)(L/s)^{1/n_0}$ and R_t are known, the *V-I* curve, and hence I_c and *n*-value, can be calculated. The term $(1-f)(L/s)^{1/n_0}$ in eq. (2) has a physical meaning of I_c/I_{c0} in a theoretical scenario where the crack is substantial and no current shunting occurs.[14] In practice, current shunting occurs, and thus the values of $(1-f)(L/s)^{1/n_0}$ and R_t are estimated from the measured *V-I* curve.

In our previous work,[1] we applied the current shunting model to the *V-I* curves of Sample A under tension. Figure 5(a) shows typical examples of the measured *V-I* curves. "A" refers to the *V-I* curve in non-cracked state and "B" to "G" in cracked state. The *V-I* curves (solid curves) were fitted by eqs. (1) and (2), and the values of $(1-f)(L/s)^{1/n_0}$ and R_t were obtained as shown in Figs. 5(b) and (c), respectively. To examine the reproducibility of the experimental results with these values of $(1-f)(L/s)^{1/n_0}$ and R_t, *V-I* curves were calculated from eqs. (1) and (2). The calculated *V-I* curves (dotted curves, Fig. 5(a)), satisfactorily reproduce the measured curves in wide range of the extent of cracking, even though this complex behavior is simply approximated in this model.

The current transported by the ligament, I_b, is calculated by $I_{c0}(1-f)(L/s)^{1/n_0}[V_b/(E_c L)]^{1/n_0}$ and the shunting current,

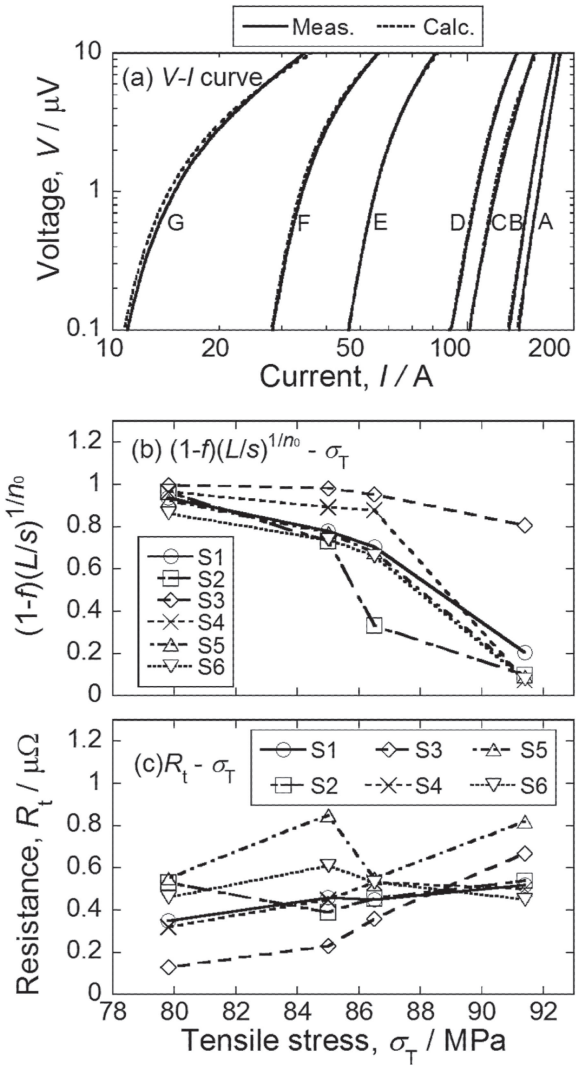

Fig. 5 Results for applying the current shunting model to the experimental results for Sample A.[1] (a) Typical examples of measured *V-I* curves (solid curves) and *V-I* curves (dotted curves) calculated by substituting the estimated values of $(1-f)(L/s)^{1/n_0}$ and R_t into eqs. (1) and (2). "A" refers to the *V-I* curve measured at $\sigma_T = 69.9$ MPa where no crack was formed. "B", "C", "D", "E", "F", and "G" refer to the *V-I* curves of S2 at $\sigma_T = 79.8$ MPa, S2 at $\sigma_T = 85.0$ MPa, S6 at $\sigma_T = 86.5$ MPa, S2 at $\sigma_T = 91.6$ MPa, S1 at $\sigma_T = 91.6$ MPa, and S6 at $\sigma_T = 91.6$ MPa in the cracked region, respectively. (b) Values of $(1-f)(L/s)^{1/n_0}$ and (c) values of R_t obtained from the *V-I* curves in the cracked region.

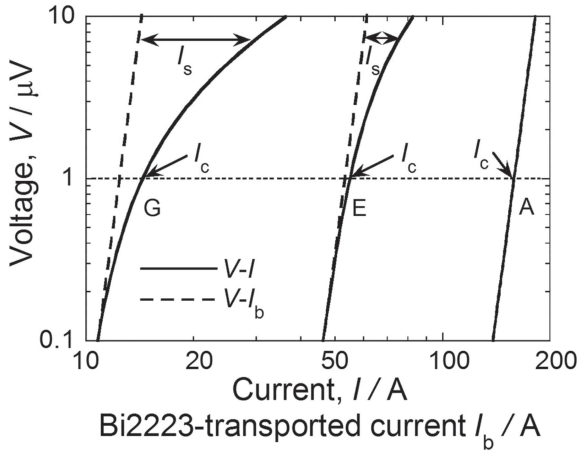

Fig. 6 Examples of the calculated *V-I* and *V-I*$_b$ curves on a logarithmic scale, showing the increase in shunting current with increasing V when cracking occurs. "A", "E", and "G" in this figure correspond to "A", "E", and "G" in Fig. 5(a), respectively.

I_s, is calculated by V_b/R_t. Figure 6 shows examples of the calculated *V-I* and *V-I*$_b$ curves on a logarithmic scale, together with the relationship among I, I_b, and I_s. "A", "E" and "G" in the figure correspond to "A", "E" and "G" in Fig. 5(a). Because "A" is not cracked, I is equal to I_b, and I_s is zero for the whole range of V. The difference between I and I_b is equal to I_s $(= I - I_b)$ in "E" and "G".

The results in Figs. 5 and 6 show the following behavior.

(1) The $(1-f)(L/s)^{1/n_0}$ decreases with increasing applied stress owing to the increased crack extension decreasing the area fraction of the ligament at higher stresses. The cracking behavior of sections S1 to S6 is different, resulting in the wide distribution of ligament area (Fig. 5(b)). R_t also varies with applied stress, namely with crack evolution. Similar to $(1-f)(L/s)^{1/n_0}$, the R_t values of S1 to S6 differ because of the difference in damage evolution behavior. The distribution of R_t is wide, in the range of 0.2–0.8 μΩ with an average around 0.5 μΩ (Fig. 5(c)).

(2) The shunting current, I_s $(= I - I_b)$, increases with increasing V in cracked "E" and "G" (Fig. 6). This affects I_c and n-value as follows. I_c is defined as $I_c = I_b + I_s$ at $V = V_c = 1$ μV, as indicated with the arrows (Fig. 6). At 1 μV, a small shunting current, I_s, develops. This means that I_s increases I_c slightly from I_b. The n-value in this work is taken as an index, n, of $V \propto I^n$ in the voltage range of $V = 0.1$–10 μV. I_s is very low at $V = 0.1$ μV and very high at $V = 10$ μV. This behavior causes large curvature in the *V-I* curve, decreasing the n-value (Fig. 6).

2.2 Calculation of n-I_c relation

Based on our results, the current shunting model was used to derive the n-I_c relation directly. As shown in Section 2.1, R_t varies with crack extension and it differs among the test pieces owing to the differences in damage evolution, and it is in the range of 0.2–0.8 μΩ. For $R_t = 0.5$ μΩ, $(1-f)(L/s)^{1/n_0} = 0.05, 0.2, 0.4, 0.6, 0.8, 0.95$, $I_{c0} = 158$ A, and $n_0 = 17$ (average values of I_{c0} and n-value in the non-cracked state obtained from Fig. 1(a)), the *V-I* curves can be calculated (Fig. 7(a)), showing the effect of $(1-f)(L/s)^{1/n_0}$ on the *V-I* curve at a given R_t-value. As the area fraction, $(1-f)$, of the ligament decreases with the increase of the crack area fraction, f, the *V-I* curve shifts to a lower current region and the curvature of the *V-I* curve increases.

The effect of R_t on the *V-I* curve is shown in Fig. 7(b), where the calculated *V-I* curves for the values of $(1-f)(L/s)^{1/n_0} = 0.5$, $I_{c0} = 158$ A, $n_0 = 17$, and $R_t = 0.2$ (dotted curve), 0.5 (broken curve), and 1.0 μΩ (long dashed short dashed curve) are presented. The *V-I* curve tends to be curved more for lower R_t values and the n-value decreases for decreasing R_t. In addition, the critical current I_c at $V = V_c = 1$ μV increases slightly with decreasing R_t. Thus, for the n-I_c relation, the n-value decreases and the I_c value increases as R_t decreases, resulting in a sharper decrease in n-value as I_c decreases for lower R_t values.

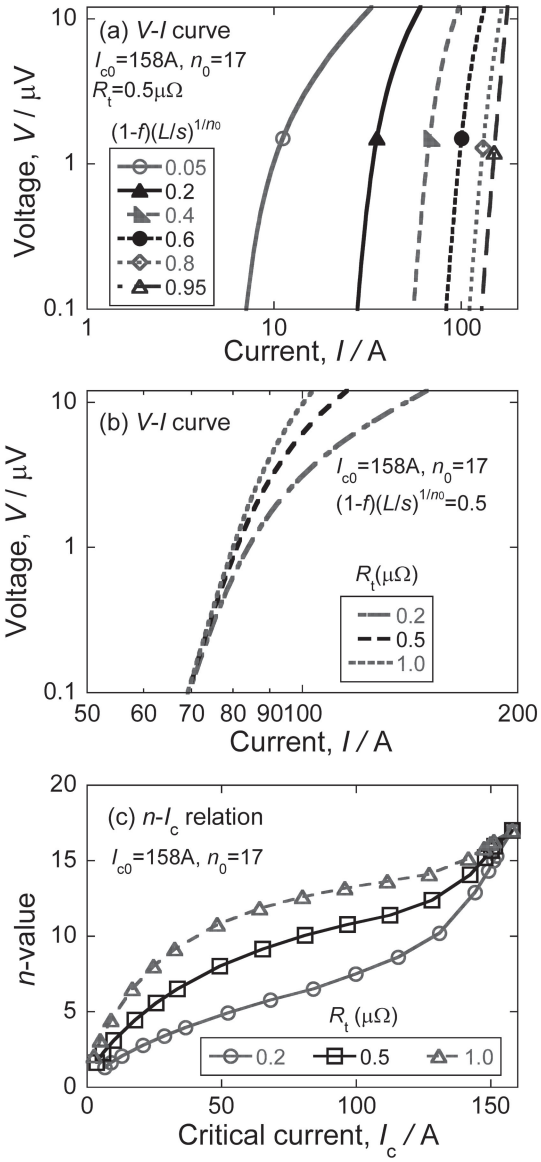

Fig. 7 Examples of the calculated *V-I* curves and *n*-I_c relation. (a) *V-I* curves calculated with eqs. (1) and (2) with $I_{c0} = 158$ A, $n_0 = 17$, $R_t = 0.5\,\mu\Omega$, and $(1-f)(L/s)^{1/n_0} = 0.05$, 0.2, 0.4, 0.6, 0.8, and 0.95. (b) *V-I* curves calculated with eqs. (1) and (2) with $(1-f)(L/s)^{1/n_0} = 0.5$, $I_{c0} = 158$ A, $n_0 = 17$, and $R_t = 0.2$ (dotted curve), 0.5 (broken curve), and $1.0\,\mu\Omega$ (long dashed short dashed curve). (c) *n*-I_c relation calculated for a wide $(1-f)(L/s)^{1/n_0}$ range and $R_t = 0.2$, 0.5, and $1.0\,\mu\Omega$ at $I_{c0} = 158$ A and $n_0 = 17$.

From the calculated *V-I* curves, we obtain (I_c, n) values for a given set of $[(1-f)(L/s)^{1/n_0}, R_t]$ values for $I_{c0} = 158$ A and $n_0 = 17$. Figures 5(a) and (b) show that the values of both of $(1-f)(L/s)^{1/n_0}$ and R_t are widely distributed owing to the difference in cracking behavior. To describe the *n*-I_c relation for this distribution, it is necessary to calculate *V-I* curves for a wide range of $[(1-f)(L/s)^{1/n_0}, R_t]$ values. In the present work, because $(1-f)(L/s)^{1/n_0}$ plays a dominant role in determining I_c,[1,11,12,14,15] this value is varied in the range of 0.025–1, which produces almost the whole range of I_c (0–I_{c0}). For example, many sets of (I_c, n) values can be obtained from the wide variety of *V-I* curves calculated from eqs. (1) and (2) using a wide range of $(1-f)(L/s)^{1/n_0}$ values (0.025–1) and $R_t = 0.2$, 0.5, and $1.0\,\mu\Omega$. From the sets of (I_c, n) values, *n*-I_c relations for $R_t = 0.2$, 0.5 and $1.0\,\mu\Omega$ can be constructed (Fig. 7(c)). In this example, the *n*-value decreases sharply as I_c decreases for low R_t values owing to the higher I_s at low R_t values.

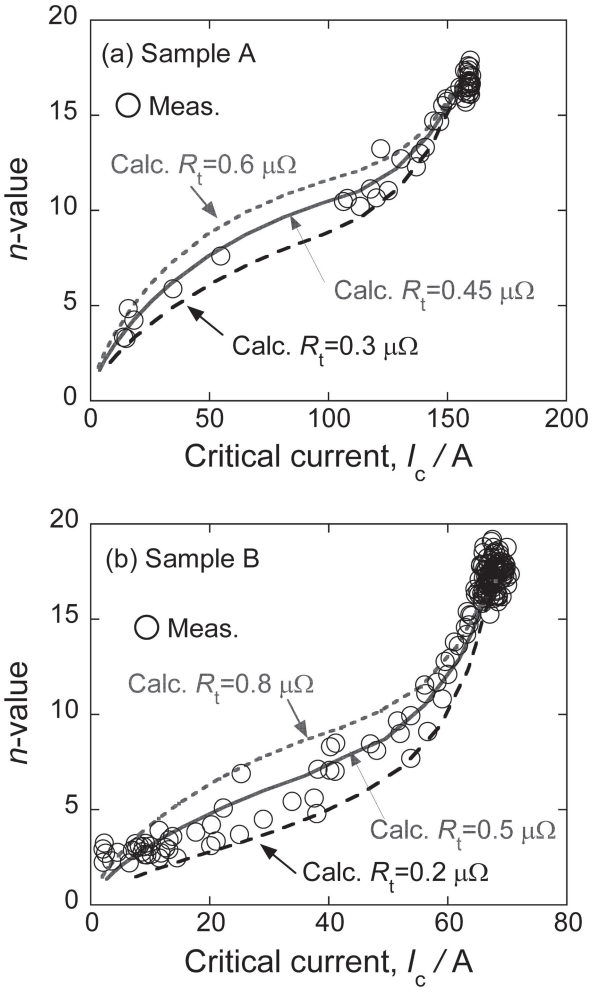

Fig. 8 Comparison of the calculated upper (dotted curve) and lower (broken curve) bounds of the *n*-I_c relation with experimental results for the BSCCO Bi2223 conductors supplied by different manufacturers. The experimental data for (a) Sample A[1)] and (b) Sample B[6)] were taken from our previous work.

Because the value of R_t is affected by the damage evolution behavior, it changes with the applied stress. The experimentally measured *n*-I_c relation is not described by a unique value of R_t. The lower and upper bounds of R_t are obtained by comparing the experimentally measured *n*-I_c diagram with the calculated *n*-I_c relations for various R_t values.

3. Measured *n*-I_c Diagram

3.1 Filamentary conductors

Figure 8(a) shows the measured *n*-I_c diagram of Sample A, taken from Fig. 1(a), and the *n*-I_c relation calculated with $R_t = 0.3$, 0.45, and $0.6\,\mu\Omega$. The experimental results are almost within the upper bound (dotted curve, $R_t = 0.6\,\mu\Omega$) and lower bound (broken curve, $R_t = 0.3\,\mu\Omega$). The R_t values giving the upper and lower bounds for the *n*-I_c diagram in Fig. 8(a) were similar to the range of R_t values (0.2–$0.8\,\mu\Omega$) obtained from the fitting of the measured *V-I* curves

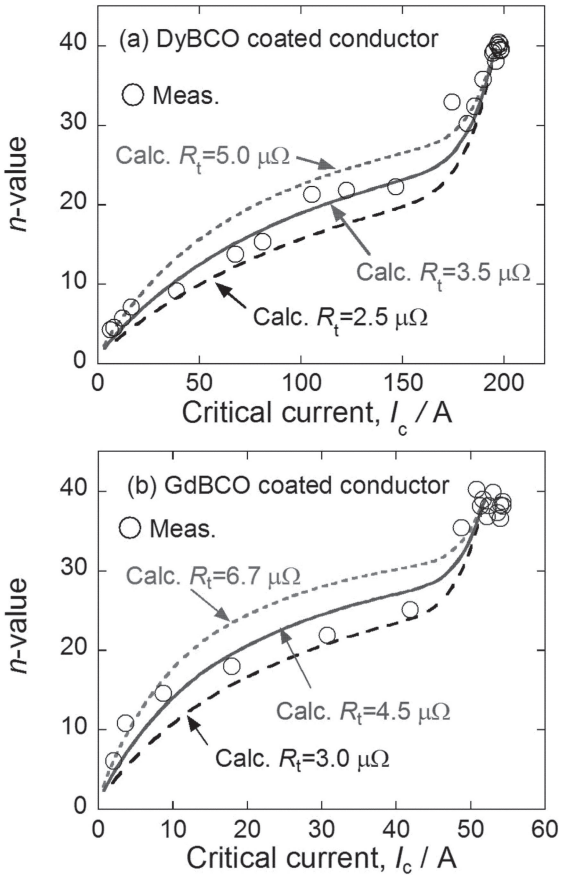

Fig. 9 Comparison of the calculated upper (dotted curve) and lower (broken curve) bounds of the n-I_c relation with experimental results for (a) DyBCO and (b) GdBCO coated conductors. The experimental data for DyBCO were taken from our previous work,[11] and that for GdBCO were taken from Ref. 16).

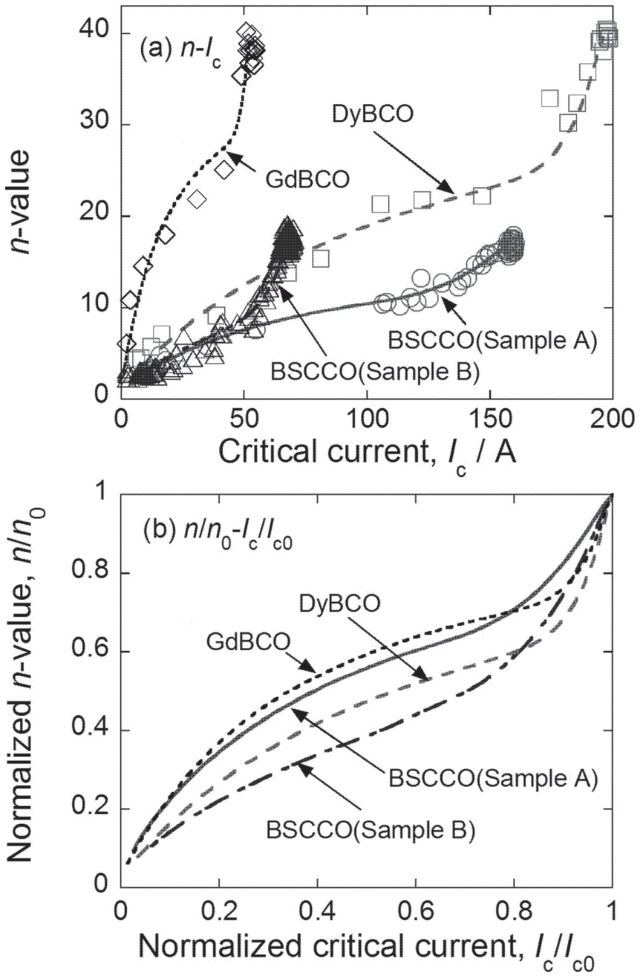

Fig. 10 (a) n-value as a function of I_c and (b) n/n_0 as a function of I_c/I_{c0}. The data for the n-I_c relation and the curves drawn through the data points in (a) were taken from Figs. 8 and 9. The curves describing n-I_c relation satisfactorily in (a) were converted to the n/n_0-I_c/I_{c0} curves in (b) by using the values $(I_{c0}, n_0) = (158\,\text{A}, 17)$, $(68\,\text{A}, 17)$, $(196\,\text{A}, 40)$, and $(52\,\text{A}, 39)$ for Sample A, Sample B, DyBCO, and GdBCO, respectively.

(Fig. 5(c)). Thus, the experimentally measured n-I_c relation can be described with the present approach by finding the lower and upper bounds of the R_t values.

The same approach was used to describe the experimental results for Sample B (Fig. 1(b)), for which the R_t value-range is unknown. Figure 8(b) shows that the experimental results are satisfactorily described with the range of $R_t = 0.2$–$0.8\,\mu\Omega$, which is similar to that of Sample A. Our approach can be used to describe the n-I_c diagram and to estimate the lower and upper bounds of the R_t value roughly.

3.2 Coated conductors

In coated conductors, the cracks in the superconducting layer reduce the I_c and n-value[11–16] as do the collective cracks in filamentary conductors.[1] To examine the applicability of the present approach to describing the n-I_c relation in a coated conductor, it was applied to the experimental results for a DyBCO coated conductor.[11] The experimental and calculated n-I_c diagrams in Fig. 9(a) show that the experimental results are described satisfactorily by the present approach. The R_t range of the sample has been estimated to be 2–5 μΩ,[11] which is similar to the calculated range of R_t (2.5–5 μΩ).

The same approach was applied to the experimental results reported by Oguro *et al.*[16] for a GdBCO-coated conductor with a sample length of 1 cm. The experimental n-I_c relation was described satisfactorily by the R_t value range of 3–6.7 μΩ. The difference in R_t value between the coated conductors (DyBCO, GdBCO) and filamentary conductors (BSCCO) might be attributed to the difference in stabilizer (copper in DyBCO and GdBCO, and silver in BSCCO). However, further study is needed to clarify this observation because R_t is affected by the current transportation of the superconducting layer/filament, stabilizer and interface, and by the crack evolution in the superconducting layer/filament, which could raise R_t-value and also could cause interfacial debonding between the superconducting layer and stabilizer when a fracture mechanical condition is satisfied.

Figure 10 shows the correlation between the n-value and I_c, and the correlation between the normalized n-value (n/n_0) and normalized critical current (I_c/I_{c0}), where n_0 and I_{c0} are the values of n and I_c in a non-cracked state, respectively. The experimental correlation between n-value and I_c, and the calculated n-I_c relation obtained with an R_t value that gives an average n-I_c curve between the upper and lower bound curves are shown in Fig. 10(a). $R_t = 0.45\,\mu\Omega$ for Sample A (filamentary BSCCO; Fig. 8(a)), $0.5\,\mu\Omega$ for Sample B (filamentary BSCCO; Fig. 8(b)), $3.5\,\mu\Omega$ for coated DyBCO

(Fig. 9(a)), and 4.5 μΩ for coated GdBCO (Fig. 9(b)). Figure 10(b) shows the relationship between n/n_0 and I_c/I_{c0}, converted from the n-I_c curves with $(I_{c0}, n_0) =$ (158 A, 17), (68 A, 17), (196 A, 40), and (52 A, 39) for Samples A and B, and the DyBCO and GdBCO samples, respectively. The n/n_0-I_c/I_{c0} relation shows the following features. (1) In all filamentary and coated conductor samples, the shape of the n/n_0-I_c/I_{c0} curves is similar; n/n_0 decreases dramatically with decreasing I_c/I_{c0} in the region where $I_c/I_{c0} = 0.8$–1, gradually where $I_c/I_{c0} = 0.3$–0.8, and then sharply where $I_c/I_{c0} = 0$–0.3. (2) The sharper reduction in n/n_0 than that in I_c/I_{c0} in the range where $I_c/I_{c0} = 0.8$–1 is caused by the early stage of crack evolution. Even when the crack is small, the n-value is greatly reduced. This reduction is greater when n_0 is higher. (3) The n-I_c relation can be calculated as shown in Figs. 7–9. As R_t increases, I_c decreases and n increases for any crack size. Accordingly, the n-I_c curve shifts to higher n for higher R_t, For any I_c-value, the n-value increases with increasing R_t. However, the height of the n/n_0 of the n/n_0-I_c/I_{c0} relation is not in the order of R_t, and is affected by I_{c0} and n_0. For example, at $I_c/I_{c0} = 0.95$, n/n_0 for samples with low R_t values (Sample A: $R_t = 0.45$ μΩ and Sample B: $R_t = 0.5$ μΩ) are higher than those with high R_t values (DyBCO: $R_t = 3.5$ μΩ and GdBCO: $R_t = 4.5$ μΩ). For Samples A and B, n_0 was 17, whereas it was around 40 for DyBCO and GdBCO. The reduction in n in the early stage of cracking is greater for larger n_0 values, the effect of which is greater than that of the R_t value. In addition, at other I_c/I_{c0} values, the height of n/n_0 is not in the order of the R_t values. Therefore, the effect of I_{c0} and n_0 on the n/n_0-I_c/I_{c0} relation is large. It is difficult to estimate R_t directly from the n/n_0-I_c/I_{c0} relation. To estimate R_t, the present approach using the n-I_c relation is simple and convenient.

Our approach is a simple, practically useful tool for describing the experimental n-I_c diagrams of both filamentary and coated conductors. It can be used to estimate the R_t value range directly from an experimental n-I_c diagram.

4. Conclusions

(1) Collective filament-cracks in filamentary superconducting tapes reduce the cross-sectional area of the superconducting current transportable-filaments, and hence the critical current, I_c. The shunting current at the crack reduces the n-value.

(2) In cracked samples, the n-value decreases and the I_c value increases slightly as the electrical resistance in the current shunting circuit decreases.

(3) A simple approach based on a current shunting model was presented to describe the n-I_c diagram measured for existing cracks. The experimental n-I_c diagram for two BSCCO samples supplied by different manufacturers were described with the upper and lower bounds of the resistance value in the shunting circuit.

(4) The experimental n-I_c diagrams for two coated conductors fabricated by different routes were also described by the present approach. The present approach is a simple, practically useful tool for describing n-I_c diagrams of filamentary and coated conductors.

REFERENCES

1) S. Ochiai, H. Okuda, M. Sugano, K. Osamura, A. Otto and A. P. Malozemoff: Mater. Trans. **53** (2012) 1549–1555.
2) Y. Miyoshi, E. P. A. Van Lanen, M. M. Dhalléand and N. Nijhuits: Supercond. Sci. Technol. **22** (2009) 085009.
3) S. Ochiai, T. Nagai, H. Okuda, S.-S. Oh, M. Hojo, M. Tanaka, M. Sugano and K. Osamura: Supercond. Sci. Technol. **16** (2003) 988–994.
4) S. Ochiai, H. Okuda, M. Sugano, M. Hojo, K. Osamura, T. Kuroda, H. Kumakura, H. Kitaguchi, K. Itoh and H. Wada: Mater. Trans. **51** (2010) 1663–1670.
5) S. Ochiai, H. Matsubayashi, H. Okuda, K. Osamura, A. Otto and A. Malozemoff: Supercond. Sci. Technol. **22** (2009) 095012.
6) S. Ochiai, H. Okuda, M. Fujimoto, J.-K. Shin, M. Sugano, M. Hojo, K. Osamura, S. S. Oh and D. W. Ha: Supercond. Sci. Technol. **25** (2012) 054016.
7) S. Ochiai, M. Fujimoto, H. Okuda, S.-S. Oh and D.-W. Ha: J. Appl. Phys. **105** (2009) 063912.
8) S. Ochiai, M. Fujimoto, J.-K. Shin, H. Okuda, S.-S. Oh and D.-W. Ha: J. Appl. Phys. **106** (2009) 103916.
9) A. Otto, E. J. Harley and R. Marson: Supercond. Sci. Technol. **18** (2005) S308–S312.
10) Y. Fang, S. Danyluk and M. T. Lanagan: Cryogenics **36** (1996) 957–962.
11) S. Ochiai, T. Arai, A. Toda, H. Okuda, M. Sugano, K. Osamura and W. Prusseit: J. Appl. Phys. **108** (2010) 063905.
12) S. Ochiai, H. Okuda, T. Arai, S. Nagano, M. Sugano and W. Prusseit: Cryogenics **51** (2011) 584–590.
13) S. Ochiai, H. Okuda, S. Nagano, M. Sugano, S.-S. Oh, H.-S. Ha and K. Osamura: Mater. Trans. **55** (2014) 549–555.
14) S. Ochiai, H. Okuda and N. Fujii: Mater. Trans. **55** (2014) 1479–1487.
15) S. Ochiai, H. Okuda, N. Fujii and K. Osamura: Mater. Trans. **56** (2015) 381–388.
16) H. Oguro, T. Suwa, T. Suzuki, S. Awaji, K. Watanabe, M. Sugano, S. Machiya, M. Sato, T. Koganezawa, T. Machi, M. Yoshizumi and T. Izumi: IEEE Trans. Appl. Supercond. **23** (2013) 8400304.